An Integrated Focusing and Calibration Procedure for Airborne SAR Data

Othmar Frey, Erich Meier, Daniel Nüesch
Remote Sensing Laboratories, University of Zurich, Switzerland
E-mail: ofrey@geo.unizh.ch

Abstract

Topography-induced variation of radar brightness still poses a problem in terms of radiometric calibration of SAR data, which is undoubtedly an indispensable step in order to deduce bio- or geophysical parameters from amplitude images. We propose an integrated focusing and calibration procedure for airborne SAR data based on the time-domain back-projection technique. With the help of sensor position and attitude data as well as a digital elevation model (DEM) the true acquisition geometry is maintained throughout the combined focusing and calibration step. The effectiveness of the method is evaluated by means of an E-SAR L-band data set acquired over undulating terrain.

1 Introduction

Topography causes geometric and radiometric distortions in SAR images deteriorating their interpretability considerably. By contrast, end-users are most often interested in retrieving bio- or geophysical parameters from SAR data, which requires that the SAR images be not only well-focused but also that the topography-induced distortions be removed by applying appropriate geocoding and radiometric correction approaches.

For flat terrain, geocoding and radiometric correction of SAR data is rather straightforward. But in order to obtain geometrically and radiometrically corrected SAR images of mountainous areas additional knowledge about the topography and the sensor's trajectory and attitude has to be included in the processing or post-processing steps. This is in particular true for airborne SAR data, where an accurate reconstruction of the acquisition geometry and its relation to the terrain is even more crucial.

Usually, the geocoding step and radiometric corrections are applied after the SAR data have been focused in azimuth. Various well-known focusing techniques are available to transform SAR raw data into a single look complex image such as the range-Doppler [1], the chirp scaling [2] [3] or the ω-k [4] algorithm. While these algorithms perform the azimuth focusing step in the frequency domain the time-domain back-projection (TDBP) processing technique focuses the data geometrically, i.e., in the time domain.

In contrast to the frequency-domain techniques, TDBP maintains the entire geometric relationship between the sensor and the illuminated area and herewith provides a framework to incorporate geocoding and radiometric correction within the azimuth focusing step. Therefore, it has the potential to provide an accurate reconstruction of SAR data of rugged terrain not only in terms of geometric but also in terms of radiometric fidelity.

In [5] we have provided an analysis of the geolocation accuracy and the radiometric performance of this TDBP processing approach using ENVISAT/ASAR image mode data. We also have shown first results of a radiometric correction for topography-induced variation of radar brightness and the elevation antenna gain pattern (AGP) for the same sensor in [6]. The radiometric correction approach, which is based on a projection cosine and was first proposed by Ulander [7], has directly been integrated into the TDBP processor.

In this paper, we now evaluate our TDBP processing scheme with *airborne* SAR data. We show that the possibility to correct the data on a pulse-by-pulse basis makes this approach very suitable to produce radiometrically corrected images from airborne SAR data. The performance of the radiometric correction is evaluated for an L-Band data set taken by the E-SAR system of the German Aerospace Center (DLR).

2 Variation of Radar Brightness Due to Topography

Surface slopes affect SAR images of rugged terrain in two ways. They alter the radar brightness and, in addition, azimuth slopes change the polarization orientation [8]. We only discuss the first effect within this paper.

The relationship between the backscatter coefficient σ^0, which is defined as the average radar cross section per unit ground area, and the radar brightness β^0, which is defined as the average radar cross section per unit image area, can be written as [7]:

$$\sigma^0 = \beta^0 \cos \psi \, . \tag{1}$$

ψ is the projection angle, which relates the unit image area to the unit ground area. In order to be able to account for aircraft motion the following two modifications have been made with respect to the original algorithm: first, the radiometric correction is calculated for each pulse and each grid point and, second, the normal vector to the image plane is replaced by a vector $\vec{n}_I$, which is the normalized cross product of the vector $\vec{l}$ pointing in direction of the longitudinal axis of the antenna and the range vector $\vec{r}$ to a specific grid point. Thus, the projection cosine is calculated by building the dot product of $\vec{n}_I$ and the normalized surface normal vector $\vec{n}_S$. In **Figure 1** the situation is depicted for a left-looking antenna.
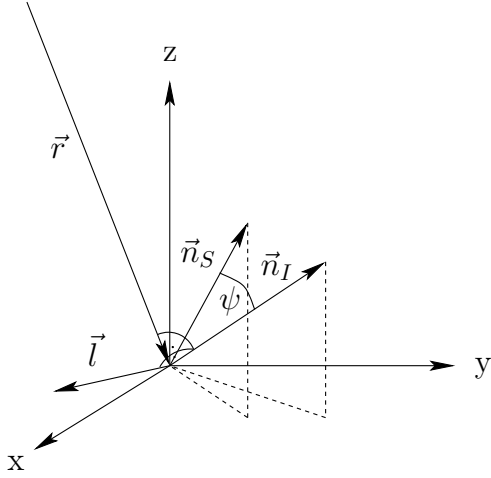

Figure 1: Geometric relationship of the projection cosine approach adapted for time-domain back-projection processing. $\vec{r}$: range vector. $\vec{l}$: direction of the longitudinal axis of the antenna. $\vec{n}_I$: normalized cross product of $\vec{l}$ and $\vec{r}$. $\vec{n}_S$: normalized surface normal vector. ψ: projection angle, which relates the unit image area to the unit ground area.

Unfortunately, the radiometric distortion, which is introduced by the elevation antenna gain pattern, could not be corrected exactly because we did not obtain the AGP of the sensor. Therefore, we omit this subject here, but we refer to [6] for a description of the topography-based AGP correction as it was applied to spaceborne SAR data.

3 System Model

For the sake of brevity we restrict ourselves to a concise description of the system model. For a more detailed derivation the reader is referred to [6]. In order to be able to back-project the data directly to a three-dimensional reconstruction grid consisting of the grid points $\vec{r}_i$ the back-projected signal s is expressed as a function of the grid point $\vec{r}_i$:

$$s(\vec{r}_i) = \sum_{j=a(\vec{r}_i)}^{b(\vec{r}_i)} \Big[g(|\vec{r}_i - \vec{r}_{S_j}|, \vec{r}_{S_j}) \\ \cdot |\vec{r}_i - \vec{r}_{S_j}| \cdot \exp(j2k_c|\vec{r}_i - \vec{r}_{S_j}|) \Big], \tag{2}$$

where a and b are the indices of the first and last sensor position, respectively, the echo of which still contributes to the grid position $\vec{r}_i$. This means that we sum up the contributions of the range-compressed two-way response $g(.)$ from those sensor positions $\vec{r}_{S_j}$ which build the synthetic aperture for the grid position $\vec{r}_i$. **Figure 2** depicts a sketch of the situation containing the relevant geometric elements. Note that a and b vary as a function of the grid position $\vec{r}_i$. Introducing the projection cosine term, which is a function of the projection angle $\psi(\vec{r}_i, \vec{r}_{S_j})$, yields:

$$s(\vec{r}_i) = \sum_{j=a(\vec{r}_i)}^{b(\vec{r}_i)} \Big[\cos(\psi(\vec{r}_i, \vec{r}_{S_j})) \cdot g(|\vec{r}_i - \vec{r}_{S_j}|, \vec{r}_{S_j}) \\ \cdot |\vec{r}_i - \vec{r}_{S_j}| \cdot \exp(j2k_c|\vec{r}_i - \vec{r}_{S_j}|) \Big]. \tag{3}$$

Equations (2) and (3) build the basis of the TDBP algorithm as it is applied to the data presented in this paper. Since the actual signal is sampled at discrete points in time an appropriate interpolation algorithm is implemented to retrieve the range-compressed data at the correct range distances.
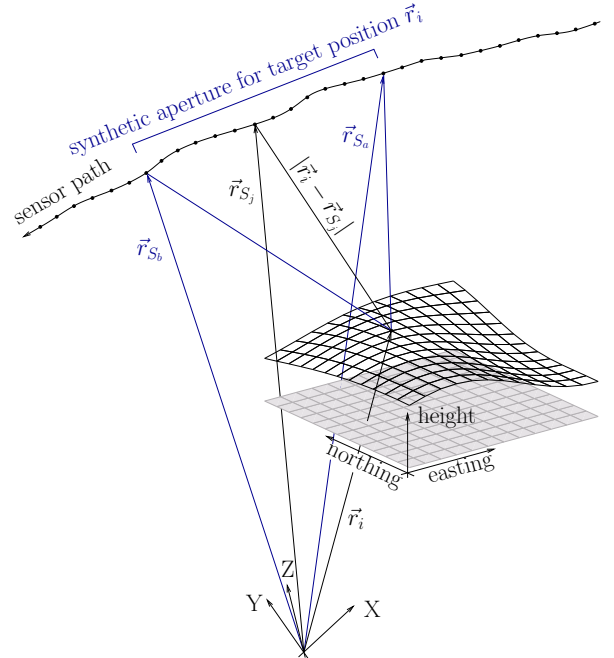

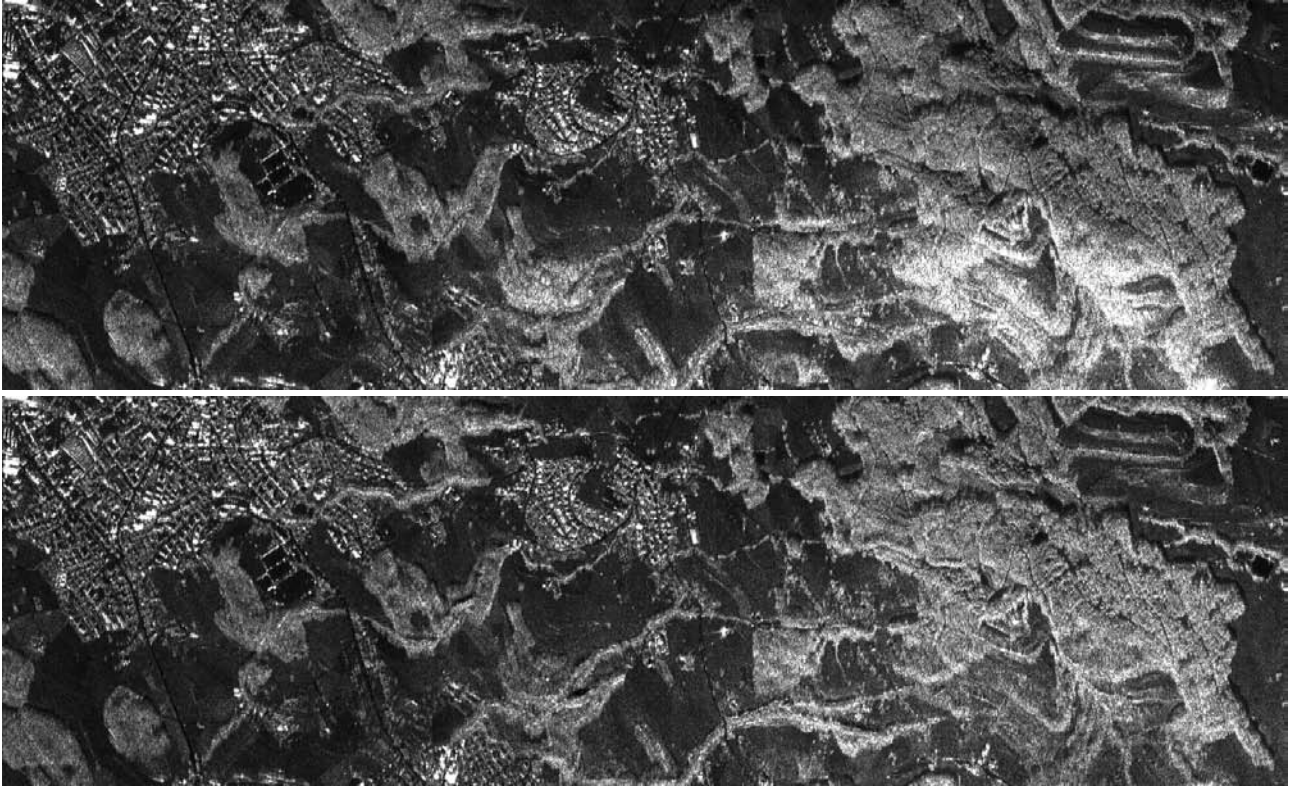**Figure 2:** Schematic view of the acquisition / reconstruction geometry.

Figure 3: ESAR L-Band HH image focused and geocoded to Swiss map coordinates (Easting / Northing) by time-domain back-projection. Upper image: without radiometric correction. Lower image: radiometrically corrected for topography-induced variation of radar brightness.

4 Data

We tested the presented processing and calibration approach using a horizontally polarized L-Band data set, which had been taken by the airborne E-SAR system of the German Aerospace Center (DLR) in 2003. The scene covers a hilly area of 4.95 km x 1.5 km size situated to the east of Zurich, Switzerland. The mean flying altitude was 3993 m above sea level whereas the terrain level varies between 560 m and 1115 m. Flying approximately towards east the sensor was looking to the left with a central elevation angle of 50° with respect to the body frame of the aircraft.

The terrain height information is provided by a highly accurate digital elevation model (DEM), which was derived from airborne laser scanning data acquired by the Falcon II system of TopoSys (http://www.toposys.com). Originally, the DEM has a pixel spacing of 1 m and a height accuracy of about 10 cm in non-forested areas. In order to meet the sampling constraints given by the bandwidth and pulse repetition frequency of the E-SAR L-Band antenna the DEM was resampled to a spacing of 0.5 m in eastern direction by cubic spline interpolation.

After preprocessing and range-compression the SAR data were processed directly to this reconstruction grid in Swiss map coordinates using the TDBP algorithm.

5 Experimental Results

The range-compressed SAR data were processed to the reconstruction grid by TDBP, once without and once with the correction for topography-induced radiometric distortion (see **Figure 3**). Since the data were focused on the digital elevation model, the images are given in map coordinates (Easting/Northing).

In the eastern part of the scene, where the terrain undulations increase, the improvement achieved by the radiometric correction is most apparent.

The effectiveness of the radiometric correction is validated by verifying the dependence of the average backscatter coefficient on the local incidence angle. This quality control is based on the assumption that the average backscatter coefficient remains constant for all local incidence angles, an assumption, which is only valid for relatively homogeneous scenes. Therefore, we only use the eastern third of the scene for our analysis. In this part of the scene, there are only very few disturbing built-up areas and, in addition, the terrain undulation is most prominent.

The data have been subdivided into 50 classes of local incidence angles for each of which the average backscatter coefficient has been calculated. In **Figure 4** the average backscatter coefficient of each class is plotted against the corresponding local incidence angle for both, uncorrected

and radiometrically corrected data. All class intervals are of identical size - this implies that the number of elements per class depends on the frequency distribution of the local incidence angles. The relative frequency of occurrence for the local incidence angle is also plotted in **Figure 4**.

For a large span of local incidence angles $\theta_l \in [13^o, 80^o]$ the variation of the average backscatter coefficient is much reduced from about 12.5 dB to less than 2.5 dB after the radiometric correction. About 99 % of the backscatter values belong to classes within this interval as can be seen from the frequency distribution in **Figure 4**.

The remaining variation of about 2.5 dB is probably due to a combination of various effects such as the uncorrected elevation AGP, inaccuracies in the DEM, differences between the DEM and the actual, illuminated surface in forested areas, and topography dependent surface characteristics. Further, there are remaining radiometric anomalies which stem from shadow and layover regions. In this scene, layover and shadow only occur in forested areas and for man-made objects.
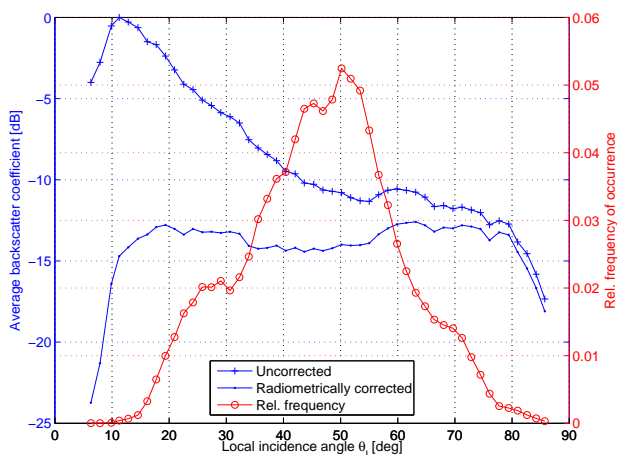

Figure 4: Dependence of the average backscatter coefficient on the local incidence angle with and without radiometric correction for topography-induced variation of radar brightness. The data have been divided into 50 classes, for each of which the average backscatter coefficient has been calculated.

6   Conclusions

An experimental framework based on time-domain back-projection processing for simultaneous azimuth focusing, geocoding and radiometric calibration of airborne SAR data has been presented. For the E-SAR L-band data set, with which our integrated focusing and calibration procedure has been tested, the variation of the average backscat-

ter coefficient is reduced from originally 12.5 dB to less than 2.5 dB for about 99 % of the pixels. A visual inspection indicates that the variation of topography-induced radar brightness is significantly reduced. However, the remaining variation of 2.5 dB is still not satisfactory. By including the elevation AGP this variation can certainly be further reduced. Aside from that, more elaborate models, such as a facet-based estimation of the local illuminated area, may have to be investigated in conjunction with the time-domain back-projection algorithm in order to improve the radiometric calibration. As can be seen from the resulting images forested areas with their inhomogeneous backscatter characteristics pose a particular challenge in terms of an accurate radiometric calibration.

References

[1] J. C. Curlander and R. N. McDonough, *Synthetic Aperture Radar - Systems and Signal Processing*. New York: John Wiley & Sons, 1991.

[2] R. K. Raney, H. Runge, R. Bamler, I. G. Cumming, and F. Wong, "Precision SAR Processing Using Chirp Scaling," *IEEE Transactions on Geoscience and Remote Sensing*, vol. 32, no. 4, pp. 786–799, 1994.

[3] A. Moreira and Y. Huang, "Airborne SAR Processing of Highly Squinted Data Using a Chirp Scaling Approach with Integrated Motion Compensation," *IEEE Transactions on Geoscience and Remote Sensing*, vol. 32, no. 5, pp. 1029–1040, 1994.

[4] C. Cafforio, C. Prati, and F. Rocca, "SAR Data Focusing Using Seismic Migration Techniques," *IEEE Transactions on Aerospace and Electronic Systems*, vol. 27, no. 2, pp. 194–207, 1991.

[5] O. Frey, E. Meier, and D. Nüesch, "A Study on Integrated SAR Processing and Geocoding by Means of Time-Domain Backprojection," in *Proceedings of the Int. Radar Symposium, Berlin*, 2005.

[6] ——, "Processing SAR data of rugged terrain by time-domain back-projection," in *SPIE Vol. 5980: SAR Image Analysis, Modeling, and Techniques X*, 2005.

[7] L. M. H. Ulander, "Radiometric slope correction of synthetic-aperture radar images," *IEEE Transactions on Geoscience and Remote Sensing*, vol. 34, no. 5, pp. 1115–1122, 1996.

[8] J.-S. Lee, D. Schuler, and T. Ainsworth, "Polarimetric SAR data compensation for terrain azimuth slope," *IEEE Transactions on Geoscience and Remote Sensing*, vol. 38, no. 5, pp. 2153–2163, 2000.